

AD 615164

MEMORANDUM

ARM-4494-ARPA

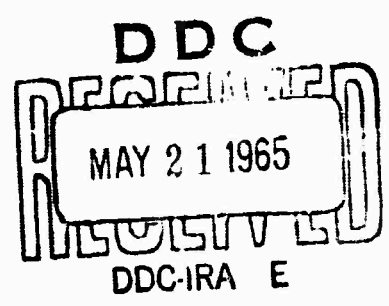
APRIL 1965

COPY	2	OF	3	19
HARD COPY	\$.2.00			
MICROFICHE	\$.0.50			

438

THE TRANSMISSION OF
 GEOMAGNETIC MICROPULSATIONS THROUGH
 THE IONOSPHERE AND LOWER EXOSPHERE

E. C. Field and C. Greifinger



PREPARED FOR:

ADVANCED RESEARCH PROJECTS AGENCY

The RAND Corporation
 SANTA MONICA • CALIFORNIA

ARCHIVE COPY

MEMORANDUM
RM-4494-ARPA
APRIL 1965

THE TRANSMISSION OF
GEOMAGNETIC MICROPULSATIONS THROUGH
THE IONOSPHERE AND LOWER EXOSPHERE

E. C. Field and C. Greifinger

This research is supported by the Advanced Research Projects Agency under Contract No. SD-79. Any views or conclusions contained in this Memorandum should not be interpreted as representing the official opinion or policy of ARPA.

DDC AVAILABILITY NOTICE

Qualified requesters may obtain copies of this report from the Defense Documentation Center (DDC).

The RAND Corporation
1700 MAIN ST. • SANTA MONICA • CALIFORNIA • 90406

Approved for OTS release

PREFACE

This report is part of RAND's continuing interest in the detection of high-altitude nuclear explosions. In particular, it is concerned with low-frequency hydromagnetic waves similar to those generated by such explosions, and which are detected by ground-current measurements at world-wide locations. In this report, we direct our attention to the response of the ionosphere to such low-frequency hydromagnetic disturbances. The purpose is to separate the effects of the medium from those of the source on the transmitted disturbance.

BLANK PAGE

SUMMARY

In this paper we consider the propagation of hydromagnetic waves at altitudes below about 2000 km. This work is an extension of a previous paper (Greifinger and Greifinger, 1965) where heights below about 500 km were considered. We treat the case of plane wave propagation in the vertical direction, and assume the geomagnetic field also to be vertical (polar propagation). Currently used models indicate that the ionosphere (the height region between about 80 and 500 km) may be reasonably represented by a constant Alfvén speed and locally exponential ion-neutral collision frequency, while the lower exosphere (the region between about 500 and 2000 km) can be adequately described by an Alfvén speed which increases exponentially with height. By using these approximate forms, the solutions of the relevant forms of the electromagnetic wave equation are expressed in terms of known functions. Analytic expressions for the magnetic transmission and reflection coefficients are derived and analyzed, and numerical results are obtained. These results, although strictly applicable only to high magnetic latitudes, compare favorably with many geographically widespread experimental data. Of particular interest is the prediction of a prominent double transmission resonance in the daytime and a single strong resonance at night. This agrees with the measurements of Maple (1959) and others. Many lesser resonances are also found. The advantage of the analytic representation is the ease of interpretation of the physical results. For example, simple expressions describing the transmission resonances found by Jacobs and Watanabe (1962) for a grounded exosphere are found to be a limiting case of the equations derived here.

CONTENTS

PREFACE	iii
SUMMARY	v
FIGURE CAPTIONS	ix
Section	
I. INTRODUCTION	1
II. PHYSICAL MODEL	4
III. THE COMPOSITE TRANSMISSION AND REFLECTION COEFFICIENTS	8
IV. SOME LIMITING CASES	15
V. NUMERICAL RESULTS AND DISCUSSION	20
REFERENCES	35

FIGURE CAPTION

- Fig. 1 - Schematic model of the ionosphere and lower exosphere.
- Fig. 2 - Magnitude of the composite magnetic transmission coefficient, $|T_B|$, for the L-mode, as a function of frequency for daytime sunspot maximum conditions. For purposes of comparison, the transmission coefficient for the grounded exosphere model of Jacobs and Watanabe, and the ionospheric transmission coefficient, $|t_B|$, are also shown.
- Fig. 3 - Magnitude of the composite magnetic transmission coefficient, $|T_B|$, and of the ionospheric transmission coefficient, $|t_B|$, for the L-mode, as a function of frequency for daytime sunspot minimum conditions. In this figure and in Fig. 2, which both correspond to daytime conditions, the composite transmission coefficient shows a prominent double resonance.
- Fig. 4 - Magnitude of the composite magnetic transmission coefficient, $|T_B|$, for the L-mode, as a function of frequency for nighttime sunspot maximum conditions. For purposes of comparison, the composite transmission coefficient for a uniform exosphere, $|T_B(\lambda = \infty)|$, and the ionospheric transmission coefficient, $|t_B|$, are also shown.
- Fig. 5 - Magnitude of the composite magnetic transmission coefficient, $|T_B|$, for the L-mode, as a function of frequency for nighttime sunspot minimum conditions. For purposes of comparison, the composite transmission coefficient for a uniform exosphere, $|T_B(\lambda = \infty)|$, and the ionospheric transmission coefficient, $|t_B|$, are also shown. This figure and Fig. 4 show that the ionospheric resonance is virtually eliminated under nighttime conditions, with only the exospheric resonances remaining.
- Fig. 6 - Magnitude of the composite magnetic transmission coefficient, $|T_B|$, and of the ionospheric transmission coefficient, $|t_B|$, for the R-mode, as a function of frequency for daytime sunspot minimum conditions. The magnitudes of the resonant peaks are much smaller than those shown in Fig. 3 for the L-mode.
- Fig. 7 - Magnitude of the composite magnetic transmission coefficient, $|T_B|$, and of the ionospheric transmission coefficient, $|t_B|$, for the R-mode, as a function of frequency for nighttime sunspot minimum conditions. The magnitudes of the resonant peaks are comparable, in this case, to those shown in Fig. 5 for the L-mode.
- Fig. 8 - Magnitude of the composite magnetic transmission coefficient for the grounded ionosphere, $|T_B(H = 0)|$, for the L-mode, as a function of frequency for daytime sunspot maximum conditions. Grounding the ionosphere has caused the lowest daytime resonance, shown in Fig. 2, to be depressed and shifted upward in frequency.

Fig. 9 - Magnitude of the composite reflection coefficient, $|R|$, and of the ionospheric reflection coefficient, $|r|$, for the L-mode, as a function of frequency for daytime sunspot maximum conditions.

I. INTRODUCTION

One of the most interesting characteristics of both natural and artificially produced geomagnetic micropulsations is the existence of narrow bands of oscillations (e.g., Maple, 1959, Tepley, 1961), or equivalently, the existence of resonant peaks in their observed energy spectra (Ness et al., 1962; Davidson, 1964, Santirocco and Parker, 1963; Smith, Provazek and Bostick, 1961). The micropulsation energy spectra depend, of course, upon the nature of the sources and the transmission properties of the ionized layers which surround the earth. The observed resonant frequencies are presumably characteristic of the transmission media and, in the absence of a detailed knowledge of the sources, provide fruitful grounds for theoretical study.

The transmission of hydromagnetic waves through regions of the ionosphere and exosphere has been studied by various workers. (In what follows the term ionosphere is used in connection with the altitude region between about 80 km and 500 km.) Francis and Karplus (1960) computed ionospheric magnetic transmission coefficients by numerically integrating the relevant differential equations, but their results did not exhibit resonances. As discussed elsewhere (Greifinger and Greifinger, 1965), this was because they did not consider sufficiently low angular frequencies. Jacobs and Watanabe (1962) considered the transmission of hydromagnetic waves through the lower exosphere (the height region between about 500 km and 2000 km), which they assumed collisionless. By dividing the lower exosphere into six uniform layers, and by assuming it to be grounded, they computed magnetic transmission coefficients which exhibit pronounced

resonances in the Pc 1 and 2 range (we use the recently suggested notation of Jacobs et al., (1964)). The lower exosphere has also been analyzed by Elliott and Hodder (1965) who used an analysis technique based on the string analogy. Prince and Bostick (1964), using a realistic, but grounded, ionosphere and exosphere have computed transmission coefficients which exhibit resonances falling mainly in the Pc 1 and 2 categories. Their method was to divide the ionized regions into a large number of uniform layers and to proceed numerically.

The purpose of the present paper is to consider theoretically the transmission of micropulsations through the ionosphere and lower exosphere. Here, however, in addition to the approximations usually used to describe hydromagnetic wave propagation in the ionosphere and exosphere, we consider the case of vertical polar propagation and represent the ionosphere by a constant Alfvén speed and locally exponential ion collision frequency, and the lower exosphere by a collisionless region with an Alfvén speed which increases exponentially with height. The region above the lower exosphere is treated as having a uniform Alfvén speed. By using this model, the validity of which is discussed in Section II, it is possible to cast the ionospheric and exospheric wave equations into forms which are solvable in terms of known functions. In a previous paper (Greifinger and Greifinger, 1965) this was done for the ionosphere only, and analytic expressions for the ionospheric magnetic transmission and reflection coefficients were obtained and numerical results were presented. A knowledge of the contents of that paper, which we will henceforth refer to as I, will be assumed throughout the present

treatment. Here we join the exospheric and ionospheric solutions and obtain analytic expressions for the composite transmission and reflection coefficients which characterize the entire region below 2000 km or so. This procedure, which can be applied for oscillation periods in the range of about 100 sec to 1/10 sec, is described in Section III. The resulting expressions, although quite complicated, are less unwieldy than a pure numerical treatment. Further, the analytic forms which we obtain afford clear physical interpretations as to the origin of the experimentally measured transmission resonances. By using straight forward limiting processes one can obtain relatively simple expressions which describe the above mentioned cases of Jacobs and Watanabe (grounded exosphere) and of I (uniform Alfvén speed). These and other limits are discussed in Section IV. In Section V we present numerical results for several models. There it is shown that, in addition to the daytime ionospheric Pc 4 resonance (previously called Pc) found in I and attributed to the filtering effect of the ionosphere, a series of higher frequency exospheric resonances appears. These are essentially the Pc 1 and 2 resonances of Jacobs and Watanabe, albeit greatly modified by the more realistic lower boundary conditions used here. It is shown further in Section V that the grounded ionosphere model used, for example, by Prince and Bostick (1964), could result in a severe misplacing of the daytime Pc 4 resonance. Although the present treatment is strictly applicable only to vertical polar propagation (it appears that this condition could be relaxed) the computed transmission coefficients agree satisfactorily with magnetic power spectra measured at mid and low latitudes. This comparison of theory with experiment is made in Section V.

II. THE PHYSICAL MODEL

As was shown in I and as will be seen in the following Section, the parameters which govern the vertical polar propagation of hydromagnetic waves in the ionosphere are the ion radial cyclotron frequency, ω_i , the ion-neutral collision frequency, ν_i , and the Alfvén speed,

$$V_A = \frac{c|\omega_i|}{\omega_{pi}} = \frac{|B_0|}{\sqrt{4\pi N_i e M_i}}, \quad (1)$$

where c is the vacuum speed of light, ω_{pi} is the ionic plasma frequency, $|B_0|$ is the terrestrial magnetic field strength, N_i is the volume density of ion-pairs, e is the electronic charge (we assume single ionization), and M_i is the average ionic mass (typically 25 or so proton masses). In the lower exosphere the propagation is determined solely by the behavior of V_A , provided that we restrict ourselves to periods sufficiently short that collisional effects are small at heights in excess of 500 km or so. This latter requirement restricts our treatment to periods shorter than about 100 sec. It is quite reasonable to assume ω_i to be constant in the ionosphere. Thus, we wish to assign ionospheric height dependences to ν_i and V_A (or, equivalently, $[N_i M_i]^{-1/2}$) and an exospheric height dependence to V_A which, in addition to describing adequately the physical conditions of interest, render the relevant wave equations solvable. Fortunately, currently used ionospheric and exospheric models can be so represented.

In what follows we will take the height profiles of Alfvén speed used by Jacobs and Watanabe (1962) or Prince and Bostick (1964) as being representative. There, V_A is seen to be relatively constant

between the bottom of the ionosphere (some 80 km above ground level) and (depending upon the local time and sunspot conditions) an altitude of some 400-500 km. We take this latter height as being the "top" of the ionosphere. In the lower exosphere, which we take as the region between the ionosphere and some 1500-2000 km (again depending on the time and sunspot activity), V_A exhibits a dependence which is remarkably well fitted by a height-increasing exponential. Above the lower exosphere V_A again becomes quite uniform and will be taken as constant. With regard to the ion collision frequency, it was shown in I that by taking the origin at that height where $\nu_i = |\omega_i|$, and choosing the coordinate system so increasing Z corresponds to decreasing altitude, we may use

$$\nu_i = |\omega_i| e^{Z/\rho} \quad (2)$$

where ρ is a local scale height, of the order of 10 km. In order for this representation to be valid, it is only necessary for ν_i to have the form (2) within a few tens of kilometers on either side of the origin. This indeed corresponds to the actual physical situation.

For $\omega_i = 175$ rad/sec, which is the value which will be used here, the representation (2) places the origin some 130 km above the ground. Thus, our propagation model, which is shown schematically in Fig. 1, is described by the following formulae:

$Z = 130$ km	perfectly reflecting ground
$130 \geq Z \geq 50$ km	Earth-ionosphere cavity

$$50 \text{ km} \geq z \geq z_1 \quad V_A = V_0 \quad \text{ionosphere} \quad (3)$$

$$z_2 \geq z \geq z_3 \quad V_A = V_2 e^{-\frac{(z-z_2)}{\lambda}} \quad \text{lower exosphere} \quad (4)$$

$$z \leq z_3 \quad V_A = V_3 = V_2 e^{-\frac{(z_3-z_2)}{\lambda}} \quad \text{exosphere} \quad (5)$$

and by Eq. (2). The behavior of V_A at the level z_2 depends upon the local time. The data indicates that under daytime conditions $V_0 = V_2$ and V_A is continuous, but has a discontinuous derivative. At night, however, the depletion of ionization in the ionosphere causes the condition $V_0 \gg V_2$ to obtain, and the ionosphere-exosphere boundary is best characterized by a rather severe discontinuity in Alfvén speed. Apparently, at the level z_3 , it is reasonable to take V_A continuous with a discontinuous derivative at all times, as is assumed in Eq. (5). The numerical values which we shall use for these parameters, for various local times and sunspot conditions, will be tabulated in the Section containing our numerical results. We note that the propagation model shown in Fig. 1 is an extension of that used in I, where here we have included regions above the ionosphere.

In addition to the above analytic model for v_i and V_A we shall employ the same simplifying assumptions as did Francis and Karplus (1960) and as was done in I, viz.:

- i) Hydrostatic restoring forces and gravitational forces are small compared to electrostatic restoring forces and may be neglected.
- ii) Collisions between electrons and ions and collisions of neutrals with charged particles may be neglected. The

latter implies that the neutrals take no part in the mass motion.

iii) The ionosphere is still and flat.

iv) The wave normal is along the ionospheric density gradient.

These assumptions, coupled with the propagation model shown in Fig. 1, will permit an analytic representation of the micropulsation propagation.

III. THE COMPOSITE TRANSMISSION AND REFLECTION COEFFICIENTS

In paper I the propagation of hydromagnetic waves in and below the ionosphere was considered, and ionospheric magnetic transmission and reflection coefficients were derived and evaluated. Here we shall extend this previous work to include the filtering action of the lower exosphere. Although a knowledge of I is assumed we shall, for completeness, devote the first part of this Section to a very brief recapitulation of the ionospheric portion of the problem. We shall then go on to solve the wave equation in the exosphere and, by joining the ionospheric and exospheric solutions, shall obtain composite transmission and reflection coefficients.

Since we are considering vertical polar propagation, it is convenient to introduce the variables

$$E = E_x - iE_y, \quad B = B_x - iB_y \quad (6)$$

which, for a time dependence $e^{-i\omega t}$ with $\omega > 0$, describe the electric and magnetic fields of the left-hand circularly polarized wave (the L-mode). As discussed in I, the final results can be made to apply to the R-mode simply by using negative ω . Further, for hydromagnetic waves in the ionosphere,

$$(i) \quad \omega \ll |\omega_i| \ll |\omega_e|$$

$$(ii) \quad v_e \ll |\omega_e|$$

$$(iii) \quad M_e v_e \ll M_i v_i$$

where the subscript e denotes electron quantities. By using dimensionless variables (denoted by a tilde) with $|\omega_i|$ being the unit of frequency and $V_o/|\omega_i|$ the unit of length, it was shown in I that the electric field satisfies the following wave equation in the ionosphere:

$$\left(\frac{d^2}{d\tilde{z}^2} + f(\tilde{\omega}, \tilde{z}/\tilde{\rho}) \right) E = 0 \quad (7)$$

where

$$f(\tilde{\omega}, \tilde{z}/\tilde{\rho}) = \frac{\tilde{\omega} - i\tilde{\omega}^2 e^{-\tilde{z}/\tilde{\rho}}}{1 - i e^{-\tilde{z}/\tilde{\rho}}} \quad (8)$$

The form of (8) indicates that the ionosphere may be thought of as being composed of three regions which are defined as follows (these ionospheric regions should not be confused with the layers shown in Fig. 1):

- i) The Hall region, where $\tilde{\nu}_i \gg 1$ ($e^{\tilde{z}/\tilde{\rho}} \gg 1$); $f \approx \tilde{\omega}$ and E is a linear combination of the solutions $e^{\pm i\tilde{\omega} \frac{1}{2} \tilde{z}}$.
- ii) The Alfvén region, where $\tilde{\nu}_i/\tilde{\omega} \ll 1$ ($e^{\tilde{z}/\tilde{\rho}} \ll \tilde{\omega}$); $f \approx \tilde{\omega}^2$ and E is a combination of the solutions $e^{\pm i\tilde{\omega}\tilde{z}}$. Note that for very long periods, say $\omega \lesssim .05$ rad/sec, there is no Alfvén region below the lower exosphere. This will place a limitation upon the forthcoming analysis.
- iii) The transition region, which falls between the above two regions, and where no simplification of Eqs. (7) and (8) can be made.

Equation (7) may be transformed to a form of the hypergeometric equation with $u = 1 - i e^{-\tilde{z}/\tilde{\rho}}$ as an independent variable. Thus, the

transition region solution for \tilde{E} involves a superposition of hypergeometric functions, which goes to the proper limiting form in the Hall and Alfvén regions. This, in fact, provides the connection between the fields in the Alfvén region and those at the bottom of the ionosphere. By carrying out the mathematics of this connection, and by applying the boundary condition

$$\left[\frac{1}{E} \frac{dE}{d\tilde{Z}} \right]_{\tilde{Z} = \tilde{Z}_1} = - \frac{1}{H} \quad (9)$$

at the bottom of the Hall region, it was shown in I that the fields in the Alfvén region may be written

$$E(\tilde{Z}) = \frac{E(\tilde{Z}_1, \tilde{\omega})}{t_E} (e^{i\tilde{\omega}\tilde{Z}} + r e^{-i\tilde{\omega}\tilde{Z}}) \quad (10)$$

$$B(\tilde{Z}) = \frac{B(\tilde{Z}_1, \tilde{\omega})}{t_B} (e^{i\tilde{\omega}\tilde{Z}} - r e^{-i\tilde{\omega}\tilde{Z}}) \quad (11)$$

where t_E and t_B are the electric and magnetic transmission coefficients of the ionosphere, i.e., the ratio of the total fields at $Z = Z_1$ to the fields of the downcoming part of the signal in the Alfvén region. Clearly, r is the ionospheric reflection coefficient. The forms of t_E , t_B , and r were found in I to be

$$t_B = \frac{i}{\tilde{\omega} H} t_E = \frac{4}{\Gamma(1-2i\rho\tilde{\omega}) \left[(1+\tilde{\omega}^{\frac{1}{2}}) g(\tilde{\omega}^{\frac{1}{2}}, \tilde{\omega}) + (1-\tilde{\omega}^{\frac{1}{2}}) g(-\tilde{\omega}^{\frac{1}{2}}, \tilde{\omega}) \right]} \quad (12)$$

$$r = - \frac{(1-\tilde{\omega}^{\frac{1}{2}}) g(\tilde{\omega}^{\frac{1}{2}}, -\tilde{\omega}) + (1+\tilde{\omega}^{\frac{1}{2}}) g(-\tilde{\omega}^{\frac{1}{2}}, \tilde{\omega})}{(1+\tilde{\omega}^{\frac{1}{2}}) g(\tilde{\omega}^{\frac{1}{2}}, \tilde{\omega}) + (1-\tilde{\omega}^{\frac{1}{2}}) g(-\tilde{\omega}^{\frac{1}{2}}, \tilde{\omega})} \quad (13)$$

where

$$g(\tilde{\omega}^{\frac{1}{2}}, \tilde{\omega}) = \frac{(1-i\tilde{\omega}H) \Gamma(1-2i\rho\tilde{\omega}^{\frac{1}{2}})}{[\Gamma(1-i\rho\tilde{\omega}^{\frac{1}{2}}-i\rho\tilde{\omega})]^2} \exp \left\{ \frac{\pi}{2} \rho\tilde{\omega}^{\frac{1}{2}} - \frac{\pi}{2} \rho\tilde{\omega} - iZ_1\tilde{\omega}^{\frac{1}{2}} \right\} \quad (14)$$

and Γ denotes the Gamma-function. Also, so far as the functional form of g is concerned, $\tilde{\omega}^{\frac{1}{2}}$ and $\tilde{\omega}$ are treated as independent.

We now proceed to the main point of the present paper, namely to find solutions to the wave equation in the exosphere and to join these solutions with those just obtained for the ionosphere. For the purpose of this joining, we shall consider oscillation periods which are sufficiently short ($\frac{2\pi}{\omega} \lesssim 100$ sec) that E and B have the limiting forms (10) and (11) near the top of the ionosphere. For much longer periods this joining would be quite complicated, since the transition region would then extend up to or beyond the ionosphere-exosphere boundary, and the fields just beneath this boundary would have to be expressed in terms of hypergeometric functions.

According to our model shown in Fig. 1, the medium is uniform for $Z \leq Z_3$ and the hydromagnetic wave equation, subject to the above mentioned restrictions on frequency, is

$$\left(\frac{d^2}{dZ^2} \quad \quad \quad \right) \begin{pmatrix} E \\ B \end{pmatrix} = 0. \quad (15)$$

We may write

$$E(\tilde{Z}) = \frac{E(\tilde{Z}_1, \tilde{\omega})}{T_E} \left(e^{i \frac{\tilde{\omega}}{\tilde{V}_3} \tilde{Z}} + \text{Re} e^{-i \frac{\tilde{\omega}}{\tilde{V}_3} \tilde{Z}} \right) \quad (16)$$

$$B(\tilde{Z}) = \frac{B(\tilde{Z}_1, \tilde{\omega})}{T_B} \left(e^{i \frac{\tilde{\omega}}{\tilde{V}_3} \tilde{Z}} - \text{Re} e^{-i \frac{\tilde{\omega}}{\tilde{V}_3} \tilde{Z}} \right) \quad (17)$$

for $Z \leq Z_3$, where T_B, T_E and R are the composite transmission and reflection coefficients for the entire region $Z_1 \geq Z \geq Z_3$, and are to be found. The application of the induction equation at Z_1 and at $Z < Z_3$ shows that

$$T_B = \frac{i \tilde{V}_3}{\tilde{\omega} \tilde{H}} T_E \quad (18)$$

In order to connect the solutions (16) and (17) to the solutions (10) and (11), we must find the form of the wave fields in the lower exosphere. Again referring to our model, the wave equation in the region $Z_2 \geq Z \geq Z_3$ is

$$\left(\frac{d^2}{d\tilde{Z}^2} + \frac{\tilde{\omega}^2}{\tilde{V}_2^2} e^{2\left(\frac{\tilde{Z} - \tilde{Z}_2}{\tilde{\lambda}}\right)} \right) E = 0 \quad (19)$$

which, by using

$$\tilde{y} = \frac{e^{\frac{\tilde{Z} - \tilde{Z}_2}{\tilde{\lambda}}}}{\tilde{V}_2} \quad (20)$$

as an independent variable becomes

$$\left(\tilde{y}^2 \frac{d^2}{d\tilde{y}^2} + \tilde{y} \frac{d}{d\tilde{y}} + \tilde{\omega}^2 \tilde{\lambda}^2 \tilde{y}^2 \right) E = 0. \quad (21)$$

Equation (21) is of course Bessel's equation of zero order, and the electric field in the lower exosphere may be written

$$E = A(\tilde{\omega}) (J_0(\tilde{\omega} \tilde{\lambda} \tilde{y}) + D(\tilde{\omega}) N_0(\tilde{\omega} \tilde{\lambda} \tilde{y})) \quad Z_2 \geq Z \geq Z_3 \quad (22)$$

where J_0 and N_0 are the Bessel and Neumann functions, and A and D are to be determined from an application of the boundary conditions. Now, by requiring that E and $dE/d\tilde{z}$ be continuous at $\tilde{z} = \tilde{z}_2$ and $\tilde{z} = \tilde{z}_3$, and by using the forms (10), (16) and (22), four readily solvable equations for A, D, R, and T_E result. By solving these, and by using Eq. (18), we find the quantities of interest, T_B and R, to be

$$T_B = \frac{4i\tilde{V}_3 e^{i\tilde{\omega}(\frac{\tilde{z}_3}{\tilde{V}_3} - \tilde{z}_2)}}{\pi \tilde{\omega} \tilde{\lambda}} \frac{t_B}{\theta [J_0(\tilde{\omega} \tilde{\lambda} \tilde{y}_3) + iJ_1(\tilde{\omega} \tilde{\lambda} \tilde{y}_3)] - \alpha [N_0(\tilde{\omega} \tilde{\lambda} \tilde{y}_3) + iN_1(\tilde{\omega} \tilde{\lambda} \tilde{y}_3)]} \quad (23)$$

where

$$\alpha = J_0(\tilde{\omega} \tilde{\lambda} \tilde{y}_2) - i\tilde{y}_2 J_1(\tilde{\omega} \tilde{\lambda} \tilde{y}_2) - re^{-2i\tilde{\omega}\tilde{z}_2} [J_0(\tilde{\omega} \tilde{\lambda} \tilde{y}_2) + i\tilde{y}_2 J_1(\tilde{\omega} \tilde{\lambda} \tilde{y}_2)] \quad (24)$$

$$B = N_0(\tilde{\omega} \tilde{\lambda} \tilde{y}_2) - i\tilde{y}_2 N_1(\tilde{\omega} \tilde{\lambda} \tilde{y}_2) - re^{-2i\tilde{\omega}\tilde{z}_2} [N_0(\tilde{\omega} \tilde{\lambda} \tilde{y}_2) + i\tilde{y}_2 N_1(\tilde{\omega} \tilde{\lambda} \tilde{y}_2)] \quad (25)$$

and

$$R = e^{\left(2i \frac{\tilde{\omega}}{\tilde{v}_3} z_3\right)} \frac{J_0(\tilde{\omega} \tilde{\lambda} \tilde{y}_3) + GN_0(\tilde{\omega} \tilde{\lambda} \tilde{y}_3) - i[J_1(\tilde{\omega} \tilde{\lambda} \tilde{y}_3) + GN_1(\tilde{\omega} \tilde{\lambda} \tilde{y}_3)]}{J_0(\tilde{\omega} \tilde{\lambda} \tilde{y}_3) + GN_0(\tilde{\omega} \tilde{\lambda} \tilde{y}_3) + i[J_1(\tilde{\omega} \tilde{\lambda} \tilde{y}_3) + GN_1(\tilde{\omega} \tilde{\lambda} \tilde{y}_3)]} \quad (26)$$

where

$$G = - \frac{e^{i\tilde{\omega}\tilde{z}_2} [J_0(\tilde{\omega} \tilde{\lambda} \tilde{y}_2) - i\tilde{y}_2 J_1(\tilde{\omega} \tilde{\lambda} \tilde{y}_2)] - re^{-i\tilde{\omega}\tilde{z}_2} [J_0(\tilde{\omega} \tilde{\lambda} \tilde{y}_2) + i\tilde{y}_2 J_1(\tilde{\omega} \tilde{\lambda} \tilde{y}_2)]}{e^{i\tilde{\omega}\tilde{z}_2} [N_0(\tilde{\omega} \tilde{\lambda} \tilde{y}_2) - i\tilde{y}_2 N_1(\tilde{\omega} \tilde{\lambda} \tilde{y}_2)] - re^{-i\tilde{\omega}\tilde{z}_2} [N_0(\tilde{\omega} \tilde{\lambda} \tilde{y}_2) + i\tilde{y}_2 N_1(\tilde{\omega} \tilde{\lambda} \tilde{y}_2)]} \quad (27)$$

In these expressions, t_B and r are the ionospheric transmission and reflection coefficients which were defined earlier, and \tilde{y}_2 means \tilde{y} , as defined by Eq. (20), evaluated at $\tilde{z} = \tilde{z}_2$, etc. Finally, the Wronskian relation

$$J_1(\tilde{\omega} \tilde{\lambda} \tilde{y}) N_0(\tilde{\omega} \tilde{\lambda} \tilde{y}) - J_0(\tilde{\omega} \tilde{\lambda} \tilde{y}) N_1(\tilde{\omega} \tilde{\lambda} \tilde{y}) = \frac{2}{\pi \tilde{\omega} \tilde{\lambda} \tilde{y}} \quad (28)$$

was used in deriving Eqs. (23)-(27).

IV. SOME LIMITING CASES

The expressions (23) and (26) for T_B and R have been numerically evaluated for several propagation models, and the results will be given in the following Section. Prior to this, however, we shall consider some of the limiting forms of T_B and R . These limiting cases, which are much simpler than the general expressions shown above, will prove very useful in interpreting the forthcoming numerical results. Further, by considering limiting situations, it will be possible to draw conclusions regarding the origin of many of the experimentally measured transmission resonances.

Jacobs and Watanabe (1962) considered the transmission of hydromagnetic waves through a grounded lower exosphere, and obtained pronounced transmission resonances. Their model, is, in fact, a limiting case of that shown in Fig. 1. We first replace the ionosphere of our model by a perfectly conducting ground, which is accomplished by setting $\tilde{\rho} = \tilde{H} = \tilde{Z}_1 = \tilde{Z}_2 = 0$. This leads to the values

$$r = -1; \quad t_B = 2 \quad (29)$$

for the ionospheric coefficients, while α and β become simply

$$\alpha = 2J_0(\tilde{\omega} \tilde{\lambda} \tilde{y}_2); \quad \beta = 2N_0(\tilde{\omega} \tilde{\lambda} \tilde{y}_2) . \quad (30)$$

At the same time, we must also preserve the distance between \tilde{Z}_2 and \tilde{Z}_3 . Thus, since we are lowering the level of the bottom of the exosphere by an amount $|\tilde{Z}_2|$, we must also replace \tilde{Z}_3 by $\tilde{\mathcal{Z}}_3 = \tilde{Z}_3 + \tilde{Z}_2$ (remembering that $\tilde{Z}_2 < 0$). Making these changes in Eq. (23), we see that the

magnetic transmission coefficient for the grounded exosphere is given by

$$T_B \xrightarrow{\text{Grounded Exosphere}} \frac{4i\tilde{V}_3 e^{i\frac{\tilde{\omega}(\tilde{z}_3)}{\tilde{V}_3}}}{\pi \tilde{\omega} \tilde{\lambda}} \cdot [N_0(\tilde{\omega} \tilde{\lambda} \tilde{y}_2) \{J_0(\tilde{\omega} \tilde{\lambda} \tilde{y}_3) + iJ_1(\tilde{\omega} \tilde{\lambda} \tilde{y}_3)\} - J_0(\tilde{\omega} \tilde{\lambda} \tilde{y}_2) \{N_0(\tilde{\omega} \tilde{\lambda} \tilde{y}_3) + iN_1(\tilde{\omega} \tilde{\lambda} \tilde{y}_3)\}]^{-1} \quad (31)$$

where \tilde{y}_2 and \tilde{y}_3 are now referred to the new co-ordinate system.

As will be seen presently, the magnitude of T_B as given by Eq. (31)

agrees precisely with the numerical results of Jacobs and Watanabe.

The transmission resonances, which occur at the minima of the denominator, are associated solely with the filtering action of the lower exosphere.

We can deduce very simple relations for the location and magnitudes of these resonances by further simplifying Eq. (31). The numerical values for the parameters used in the model will be given in the next section, but it turns out that, generally speaking,

$$\tilde{y}_3 \sim 10^{-2} \tilde{y}_2 \quad (32)$$

and, as will be seen a posteriori, the first few exospheric resonances are so located that

$$\tilde{\omega} \tilde{\lambda} \tilde{y}_3 \ll 1. \quad (33)$$

Thus,

$$J_0(\tilde{\omega} \tilde{\lambda} \tilde{y}_3) + iJ_1(\tilde{\omega} \tilde{\lambda} \tilde{y}_3) \sim 1 \quad (34)$$

$$|N_0(\tilde{\omega} \tilde{\lambda} \tilde{y}_3) + iN_1(\tilde{\omega} \tilde{\lambda} \tilde{y}_3)| \sim \left| \frac{2}{\pi} \ln \left(\frac{2}{1.8 \tilde{\omega} \tilde{\lambda} \tilde{y}_3} \right) + \frac{2}{\pi \tilde{\omega} \tilde{\lambda} \tilde{y}_3} \right| \gg 1 \quad (35)$$

and since $N_0(\tilde{\omega} \tilde{\lambda} \tilde{y}_2)$ is of order unity or less, the first few grounded exospheric resonances are located such that

$$J_0(\tilde{\omega} \tilde{\lambda} \tilde{y}_2) \approx 0 \quad (36)$$

i.e.,

$$\tilde{\omega}_n \approx \frac{q_n}{\tilde{\lambda} \tilde{y}_2} \quad (37)$$

where q_n is the n^{th} root of J_0 ($q_1 = 2.4$, $q_2 = 5.5$, $q_3 = 8.6 \dots$).

The combination of Eqs. (32) and (37) justifies the inequality (33).

The roots of J_0 may be quite accurately located by using the

asymptotic form $J_0(x) \sim \sqrt{\frac{2}{\pi x}} \cos(x - \pi/4)$. Now reverting to

conventional units, we note that, in view of Eqs. (20) and (32), the

phase change $\Delta\varphi$ between Z_3 and Z_2 is

$$\Delta\varphi = \int_{Z_3}^{Z_2} \frac{\omega}{V_A} dZ = \lambda\omega \left[\frac{1}{V_2} - \frac{1}{V_3} \right] \approx \frac{\lambda\omega}{V_2} \quad (38)$$

which is just the argument of J_0 in Eq. (36). Thus the location of the

resonant frequencies can be written approximately

$$\cos \left(\Delta\varphi_n - \frac{\pi}{4} \right) \approx 0 \quad (39)$$

so that, in the sense of a phase integral, the grounded lower exosphere

deviates from a quarter-wave plate behavior only by the phase

factor $\pi/4$. The magnitudes of these resonant peaks are also quite easily found. By using (34), (36) and (37) in conjunction with (31) it follows that

$$|T_B(\tilde{\omega}_n)| \xrightarrow{\text{Grounded Exosphere}} \frac{4\tilde{V}_3\tilde{y}_2}{\pi q_n N_o(q_n)}. \quad (40)$$

As will be seen presently, when the exosphere is terminated upon the Alfven region of the ionosphere, rather than upon a perfect earth, the transmission peaks are shifted, broadened and depressed.

Another limit which provides useful insight is that of the uniform exosphere. This case, which is mathematically represented by taking $\tilde{\lambda} = \infty$, and hence $\tilde{y}_2 = \tilde{y}_3$ and $\tilde{V}_2 = \tilde{V}_3$, removes the filtering action of the lower exosphere and thus eliminates the exospheric resonances. In this case, by using the Wronskian relation (28), Eqs. (23) and (26) become

$$T_B \xrightarrow{\lambda = \infty} e^{i\tilde{\omega}(\frac{\tilde{Z}_3}{\tilde{V}_3} - \tilde{Z}_2)} \frac{2t_B}{1 + \tilde{y}_2 + re^{-2i\tilde{\omega}\tilde{Z}_2}(\tilde{y}_2 - 1)} \quad (41)$$

and

$$R \xrightarrow{\lambda = \infty} e^{2i\frac{\tilde{\omega}}{\tilde{V}_3}\tilde{Z}_3} \frac{\tilde{y}_2(1 + re^{-2i\tilde{\omega}\tilde{Z}_2}) - (1 - re^{-2i\tilde{\omega}\tilde{Z}_2})}{\tilde{y}_2(1 + re^{-2i\tilde{\omega}\tilde{Z}_2}) + (1 - re^{-2i\tilde{\omega}\tilde{Z}_2})}. \quad (42)$$

Since the exospheric resonances have been removed in this limit, any resonances which remain must obviously be associated with the filtering action of the ionosphere. For daytime conditions,

$\tilde{y}_2 = 1$ and $\tilde{V}_3 = 1$, so that Eqs. (41) and (42) become

$$T_B \xrightarrow[\substack{\tilde{\lambda} = \infty \\ \tilde{y}_2 = 1}]{\quad} e^{i\tilde{\omega}(\tilde{Z}_3 - \tilde{Z}_2)} t_B \quad (43)$$

$$R \xrightarrow[\substack{\tilde{\lambda} = \infty \\ \tilde{y}_2 = 1}]{\quad} e^{2i\tilde{\omega}(\tilde{Z}_3 - \tilde{Z}_2)} r \quad (44)$$

These are, of course, just the ionospheric transmission and reflection coefficients referred to the height \tilde{Z}_3 , and the resonances are consequently exactly those obtained in I. On the other hand, in the nighttime a discontinuity in Alfvén speed, and hence an impedance mismatch, arises at the height \tilde{Z}_2 . The result of this mismatch, which is rather severe, is the virtual elimination of the lowest (and, for practical purposes, only) ionospheric resonance.

The numerical results for these limits, together with those for the full expression, will be presented in the next section.

V. NUMERICAL RESULTS AND DISCUSSION

In this Section we present numerical results for the transmission and reflection coefficients for several model ionospheres and lower exospheres. These results, although obtained for polar propagation, will be compared with, and will be seen to agree well with, experimental data obtained at mid and low latitudes. The relevant parameters, which were chosen essentially to correspond to the Alfvén-speed height-profiles used by Jacobs and Watanabe (1962) or Prince and Bostick (1964) are shown in Table 1. In addition, we shall use $|\omega_i| = 175$ rad/sec and an ion-collision frequency scale height, ρ , of 10 km. These two values were shown in I to describe conditions in the ionosphere satisfactorily.

Local time and sunspot conditions	V_0 (km/sec)	V_2 (km/sec)	λ (km)	Z_2 (km)	Z_3 (km)
Day-Sunspot Max.	200	200	445	-220	-1870
Night-Sunspot Max.	5000	450	455	-370	-1950
Day-Sunspot Min.	400	400	310	-320	-1320
Night-Sunspot Min.	5000	800	280	-270	-1170

Table 1

IONOSPHERIC AND LOWER EXOSPHERIC PARAMETERS

The quantity of interest with respect to understanding the observed spectra of micropulsations is the composite transmission coefficient. Our numerical results for the magnitude of T_B for the L-mode, corresponding to the four models given in Table 1, are shown in Figs. 2-5. The R-mode transmission coefficients, for the day and night sunspot minimum models, are shown in Figs. 6 and 7. We have also shown in Figs. 2-7, for purposes of comparison, the ionospheric transmission coefficients $|t_B|$ and $|T_B(\lambda = \infty)|$. It will be recalled that for our daytime models, these two quantities become identical. Also, we have included in Fig. 2 the results obtained by taking the grounded exosphere limit considered by Jacobs and Watanabe (1962) and represented analytically by our Eq. (31).

The L-mode transmission coefficient, computed for daytime sunspot maximum conditions, but with $\tilde{H} = 0$ (grounded ionosphere) is shown in Fig. 8. The composite reflection coefficients are of limited use in interpreting experimental observations, and exhibit a generally complicated structure of sharp, narrow minima which occur near the transmission resonances. Sample curves of R and r , for daytime sunspot minimum conditions, are shown in Fig. 9.

We start by discussing the daytime cases and note, by comparing Figs. 2 and 3 with Fig. 6, that the daytime resonant structure of the transmitted signal is governed primarily by the L-mode. This would imply, at least for high latitudes, that the polarization of the daytime signals near the resonant frequencies should be nearly circular. The results shown in Figs. 2 and 3 indicate that the main conclusion drawn in I is unaffected by the inclusion of the lower exosphere. In particular the daytime Pc 4 resonance, which has

a period of many tens of seconds ($\tilde{\omega} \lesssim 10^{-3}$) and which is clearly due to the filtering action of the ionosphere, remains intact. Still considering the two daytime models, we see by comparing $|t_B|$ with $|T_B|$ in Figs. 2 and 3 that the inclusion of the lower exosphere introduces a series of higher frequency resonances falling in the lower Pc-3 to Pc 1 range. These peaks, which are clearly exospheric in origin, are a modified version of those predicted by Jacobs and Watanabe (1962). To illustrate this point we have included a plot of $|T_B|$ for a grounded exosphere (see Eq. (31)) in Fig. 2. This curve, which agrees closely with the corresponding numerical results of Jacobs and Watanabe, exhibits resonances which are larger, more narrow, and shifted in frequency from those evident in $|T_B|$ as obtained for the more accurate model.

One of the most striking features of the daytime models is that the first exospheric resonance is comparable in magnitude with that due to the ionosphere. This pronounced double-peak in the daytime spectrum is in good qualitative agreement with the two prominent daytime bands measured by several workers. Quantitatively, our computed values for the location and spacing of these two peaks agree better with the measurements of Ness, et al., (1962) and Smith, et al., (1961) than with those of Maple (1959) and Davidson (1964). Here we see that the two peaks arise in different ionized layers. There is also a series of higher frequency exospheric Pc 1 and 2 daytime resonances. The magnitude of these falls off rapidly with increasing frequency, due to the opacity of the daytime ionosphere. It is thus questionable if any but perhaps the first few of these could be easily measured.

Prince and Bostick (1964) have also computed magnetic transmission coefficients, which, over much of the spectrum, appear similar to those shown here. A major difference, however, is the absence of the experimentally measured Pc 4 daytime resonance in their work. Although this could possibly be a consequence of the fact that their vertical equatorial propagation model was different than the polar situation treated here, we feel that another likely explanation is their use of a grounded ionosphere ($H = 0$). We have shown, in Fig. 8, $|T_B|$ computed for the same daytime maximum conditions as in Fig. 2, except that H has been taken equal to zero. A comparison of these two figures shows that the assumption of a grounded ionosphere causes the first daytime resonance to be depressed and shifted to a considerably higher frequency. The cause of this behavior was discussed in I. The fact that the transmission coefficients computed by Prince and Bostick fall off with increasing frequency much faster than those shown here is due to the differences between polar and equatorial propagation.

We now discuss the nighttime transmission coefficients, which differ both qualitatively and quantitatively from those obtained for daytime conditions. One major difference, which can be seen in Figs. 4 and 5, is that the L-mode ionospheric Pc 4 resonance, which was prominent in the daytime, essentially vanishes. Since neither t_B nor $T_B(\lambda = \infty)$ (which includes the effects of the discontinuity in V_A at $\tilde{z} = Z_2$) exhibits any pronounced nighttime resonances, the resonant peaks in T_B are due to the lower exosphere. These exospheric resonances are much more pronounced at night than in the daytime. Finally, and of equal importance, Fig. 7

shows that the first few R-mode resonances are nearly identical in size and location to those for the L-mode. This is a consequence of the relative transparency of the nighttime ionosphere. Thus, while we would expect high latitude daytime signals to be nearly circularly polarized (at least at the resonant frequencies) nighttime ones would have essentially the polarization of the sources (assuming a steady state). Detailed measurements of the resonant-frequency polarization of high-latitude magnetic signals would be a useful check on the results presented here.

The resonant structure of the nighttime transmission coefficients agrees at least qualitatively with many of the experimental data. For example, we interpret the first and largest nighttime transmission peak as the single prominent nighttime band noted by Maple (1959) although the resonant frequencies computed here are perhaps twice as large as the 1/8 cps which he measured. Also, the computed nighttime increase in the magnitude of the Pc 1 and 2 resonances is in agreement with the nocturnal appearance of certain fluctuations in this frequency range (Benioff, 1960; Tepley and Amundsen, 1965). We must emphasize that the diurnal variation of the sources could be an important factor here, however. The possibility of strong daytime sources overcoming the generally poorer daytime Pc 1 and 2 transmission must, of course, also be considered.

In conclusion, our analytic, polar propagation model has yielded readily interpretable results which agree with experiment in the following respects:

- 1) A strong double daytime resonance in agreement with the measurements of Maple (1959), and others has been obtained.

- 2) A strong nighttime resonance, again in agreement with Maple, has been obtained.
- 3) The computed nocturnal prominence of the exospheric Pc 1 and 2 resonances agrees with the measured diurnal behavior of certain classes of micropulsations.

The basic structure of the micropulsation spectra is thus contained in the expressions given here. A more detailed quantitative agreement with experiment could presumably be attained by adjusting the values of the parameters used. Further, the ability to take simple limiting cases of our analytic expressions has provided physical insight with regard to the transmission and reflection processes. There are, of course, limitations in our treatment. The most severe is perhaps the restriction to polar propagation. This prevents an analysis of the latitude dependence of the transmission resonances and polarization of ground-level signals. The extension to non-polar situations does seem feasible, however, and is presently being considered.

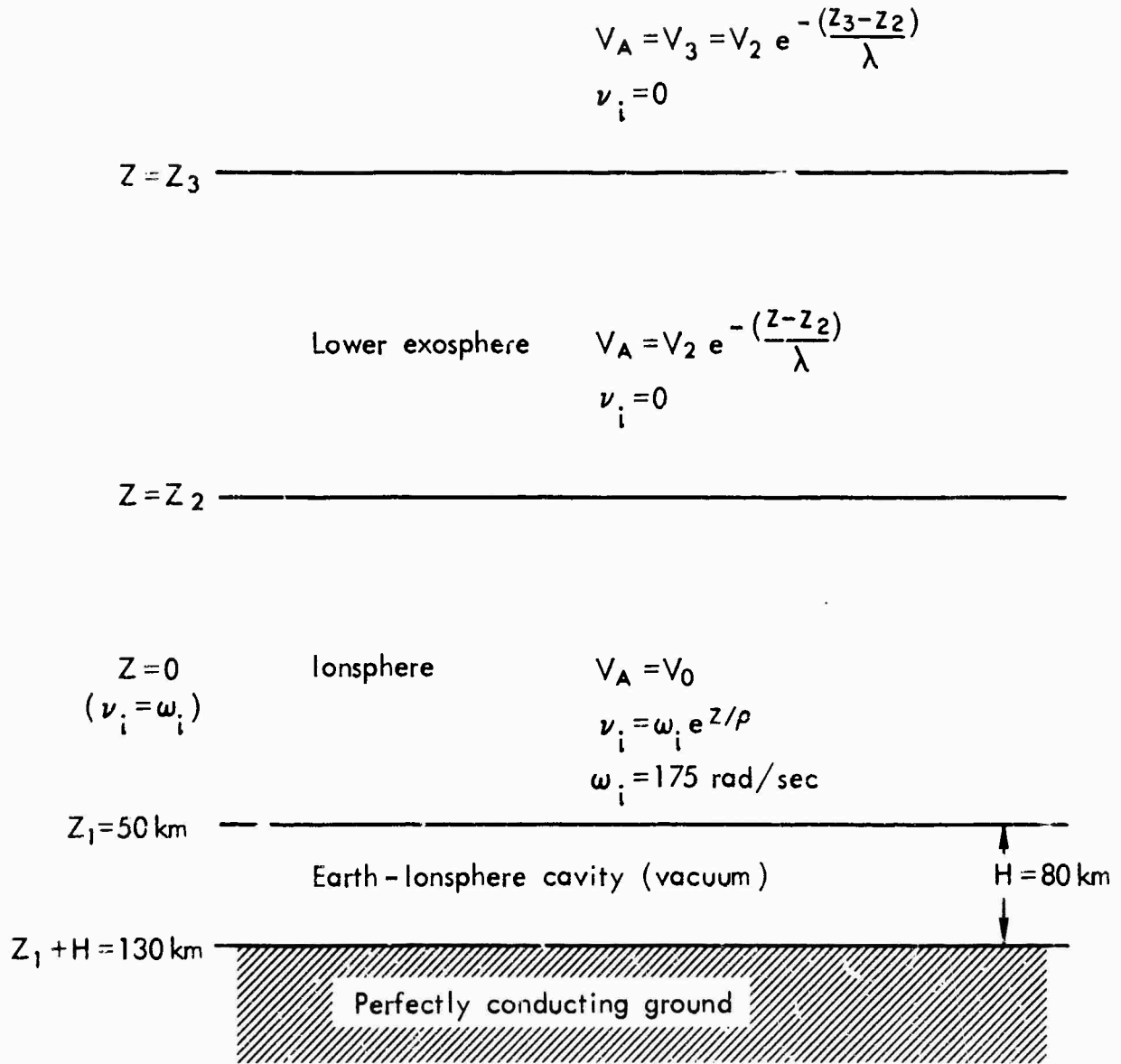


Fig. 1

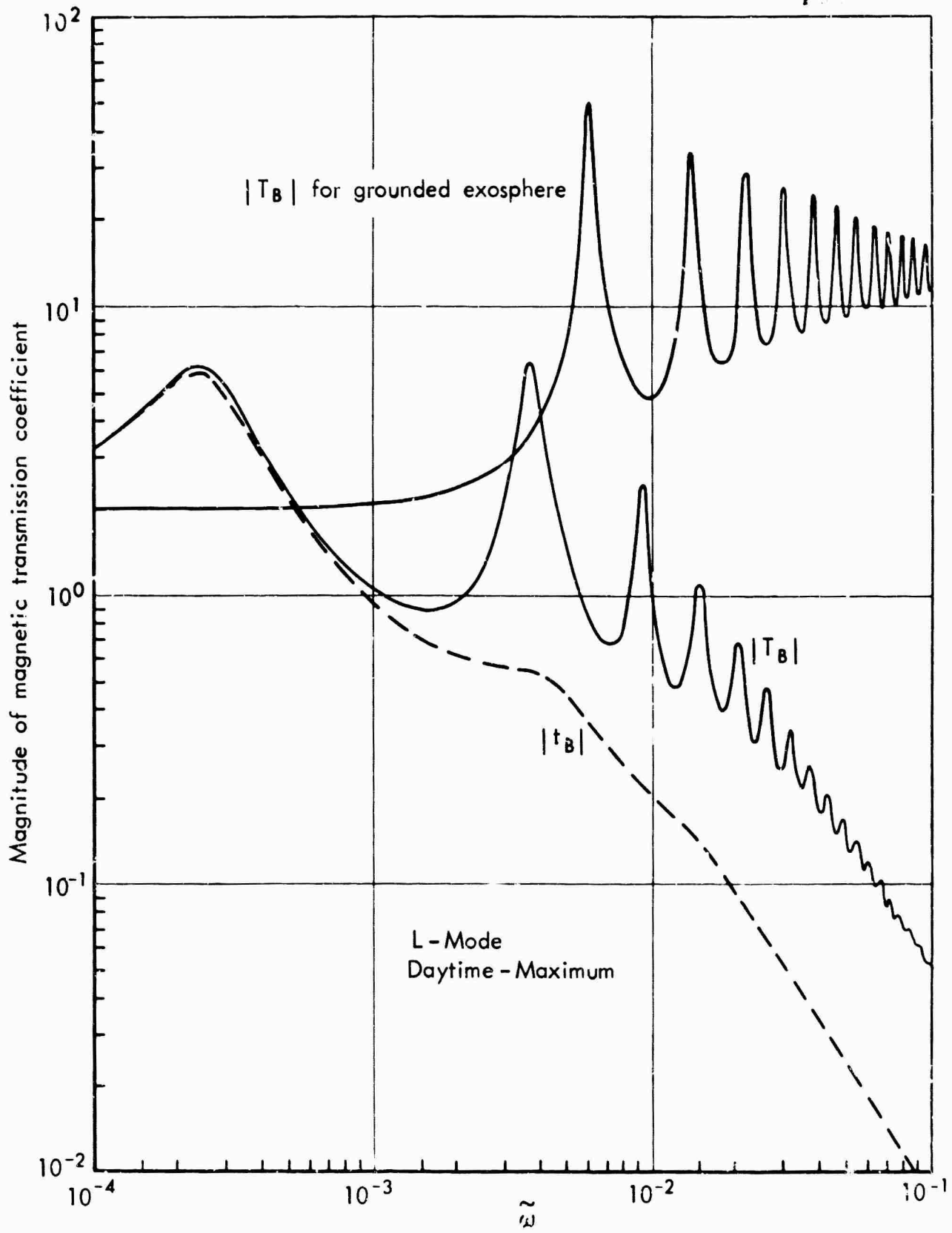


Fig. 2

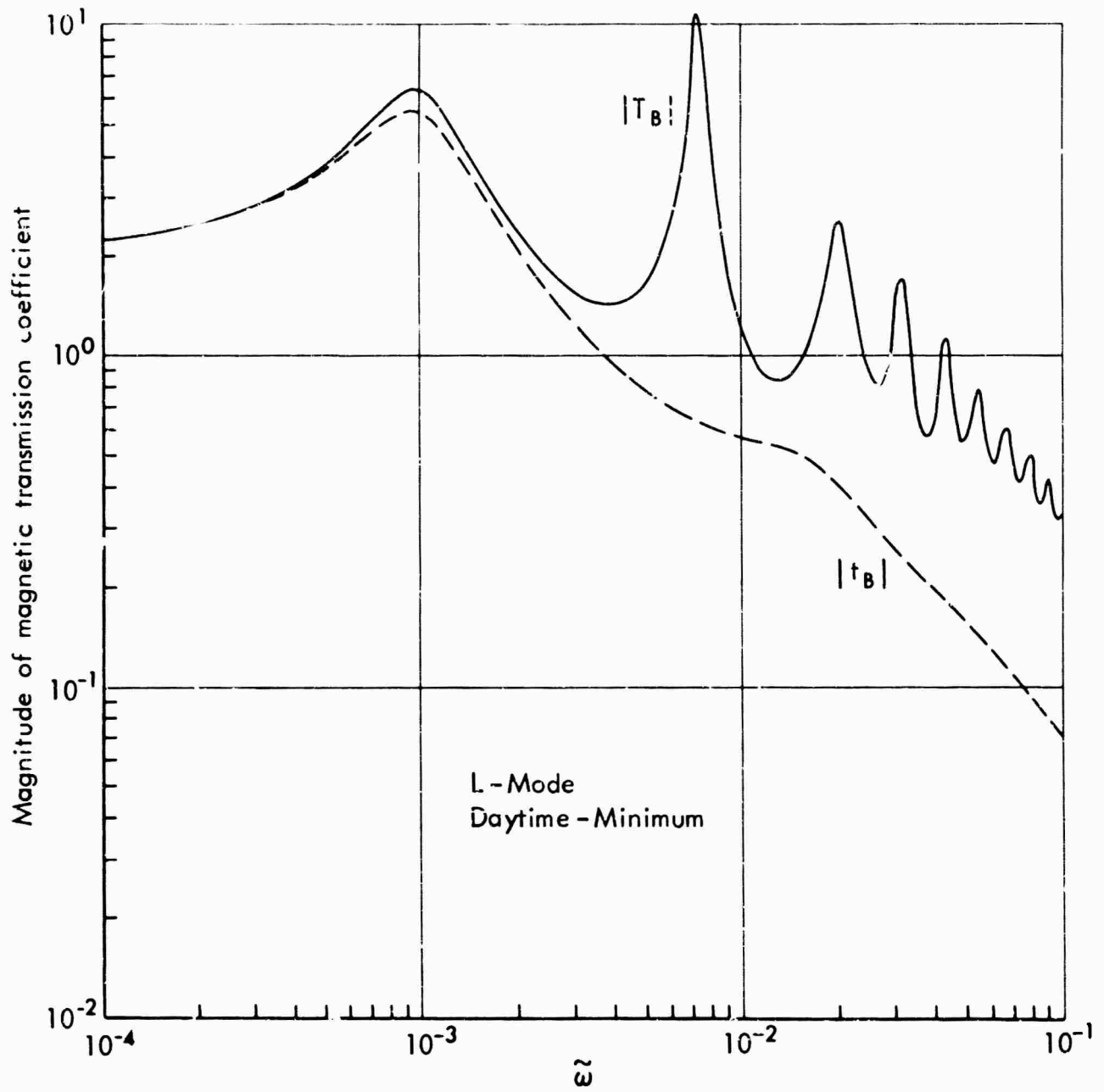


Fig. 3

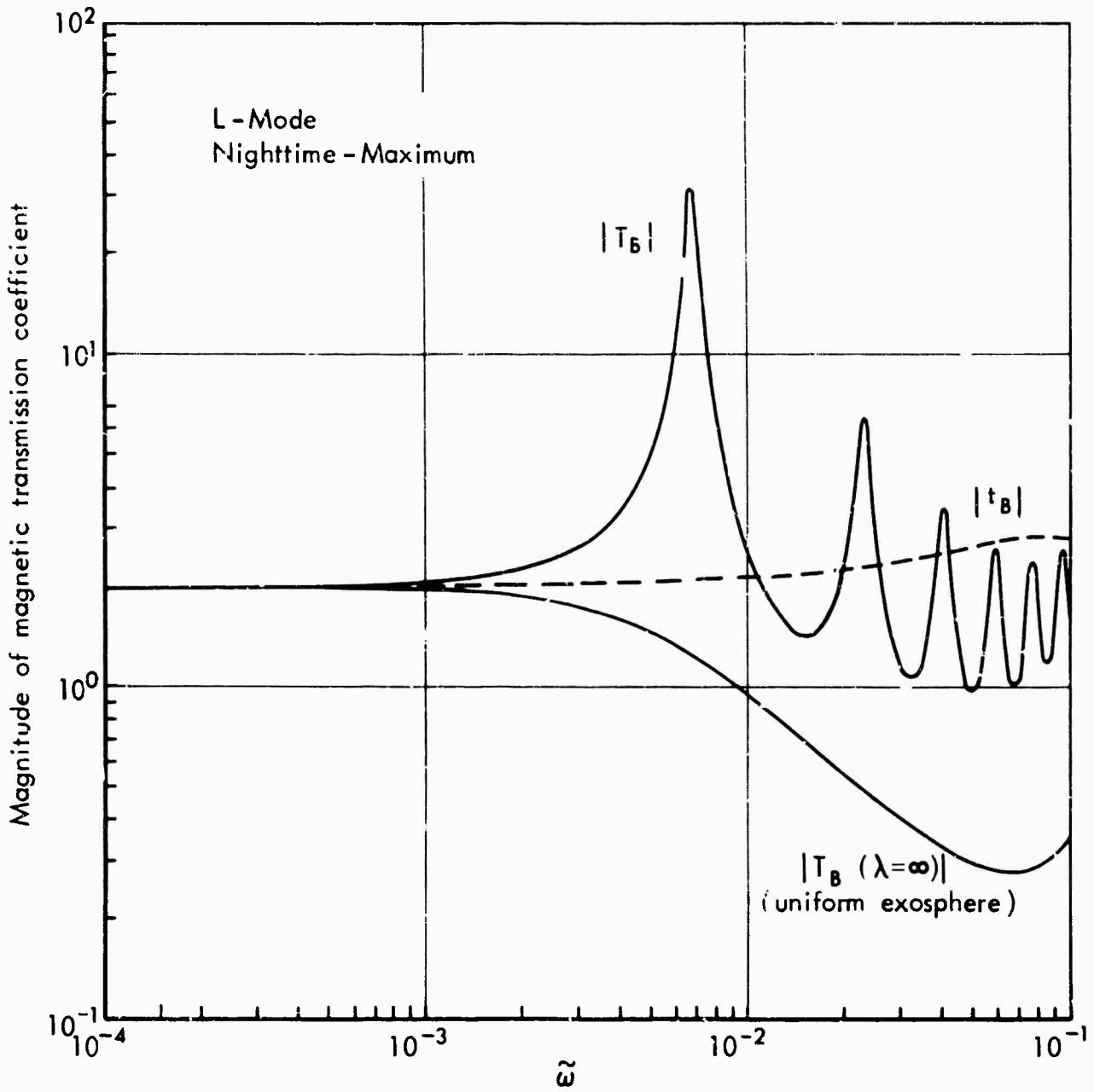


Fig. 4

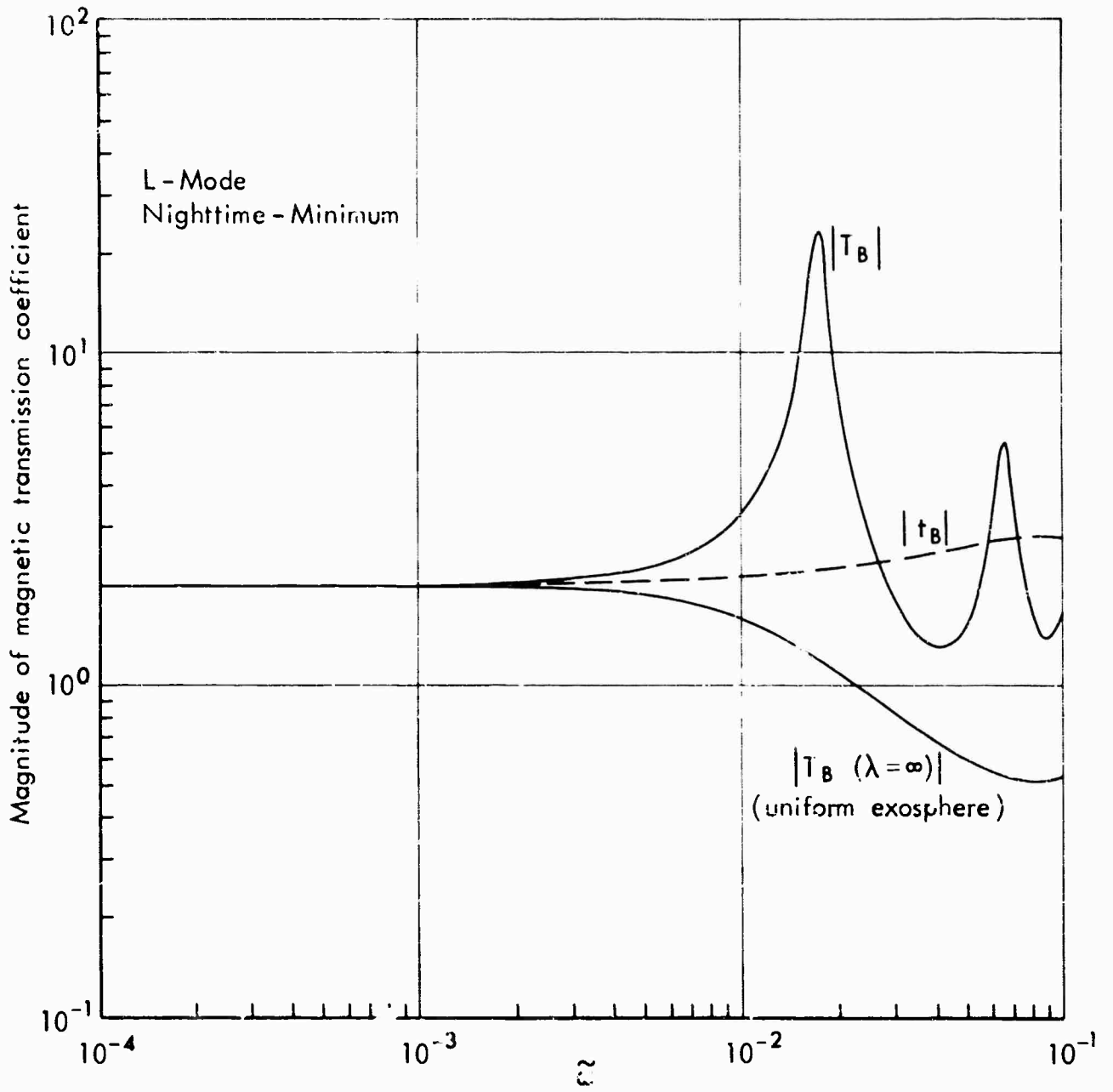


Fig. 5

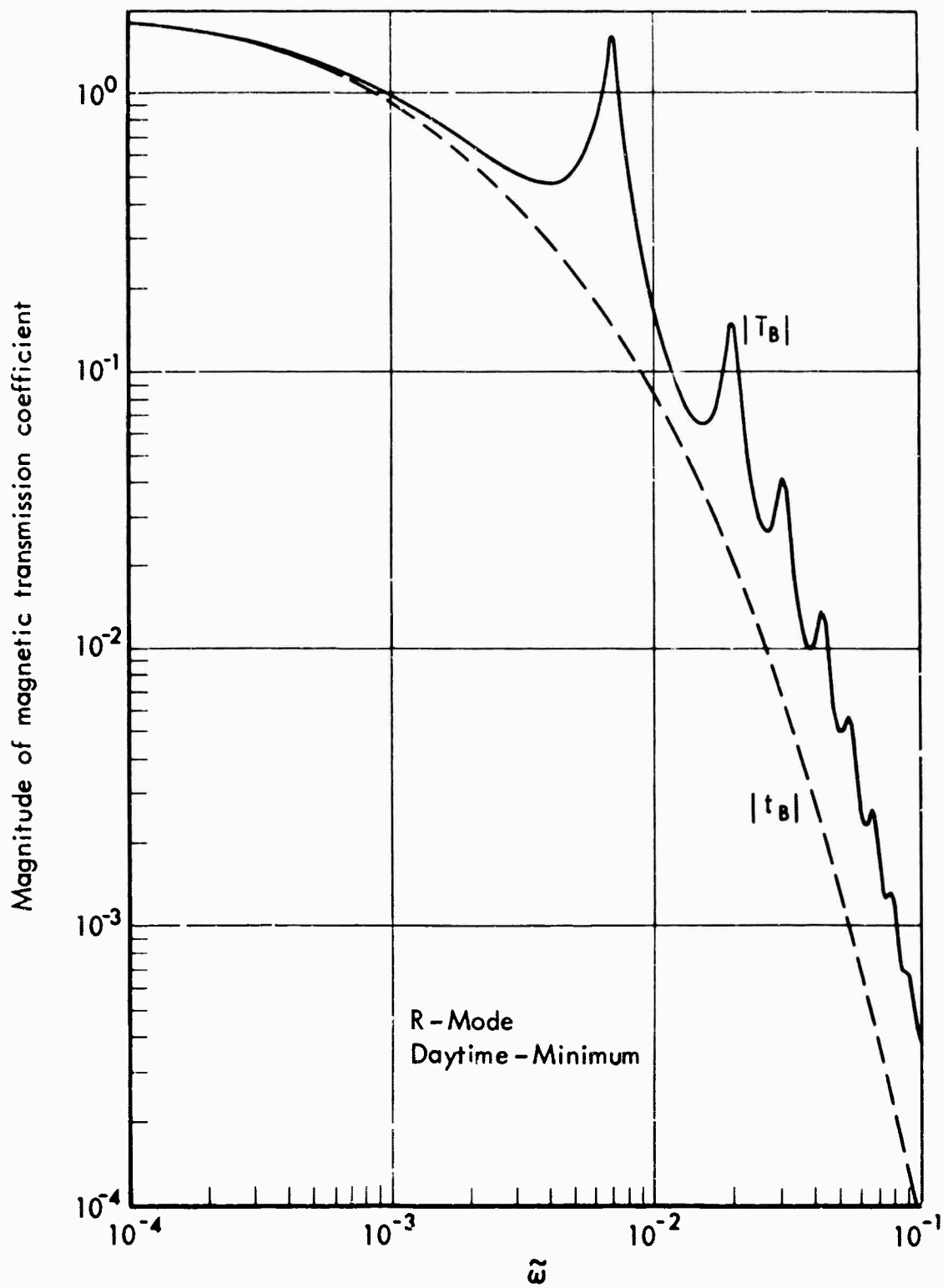


Fig. 6

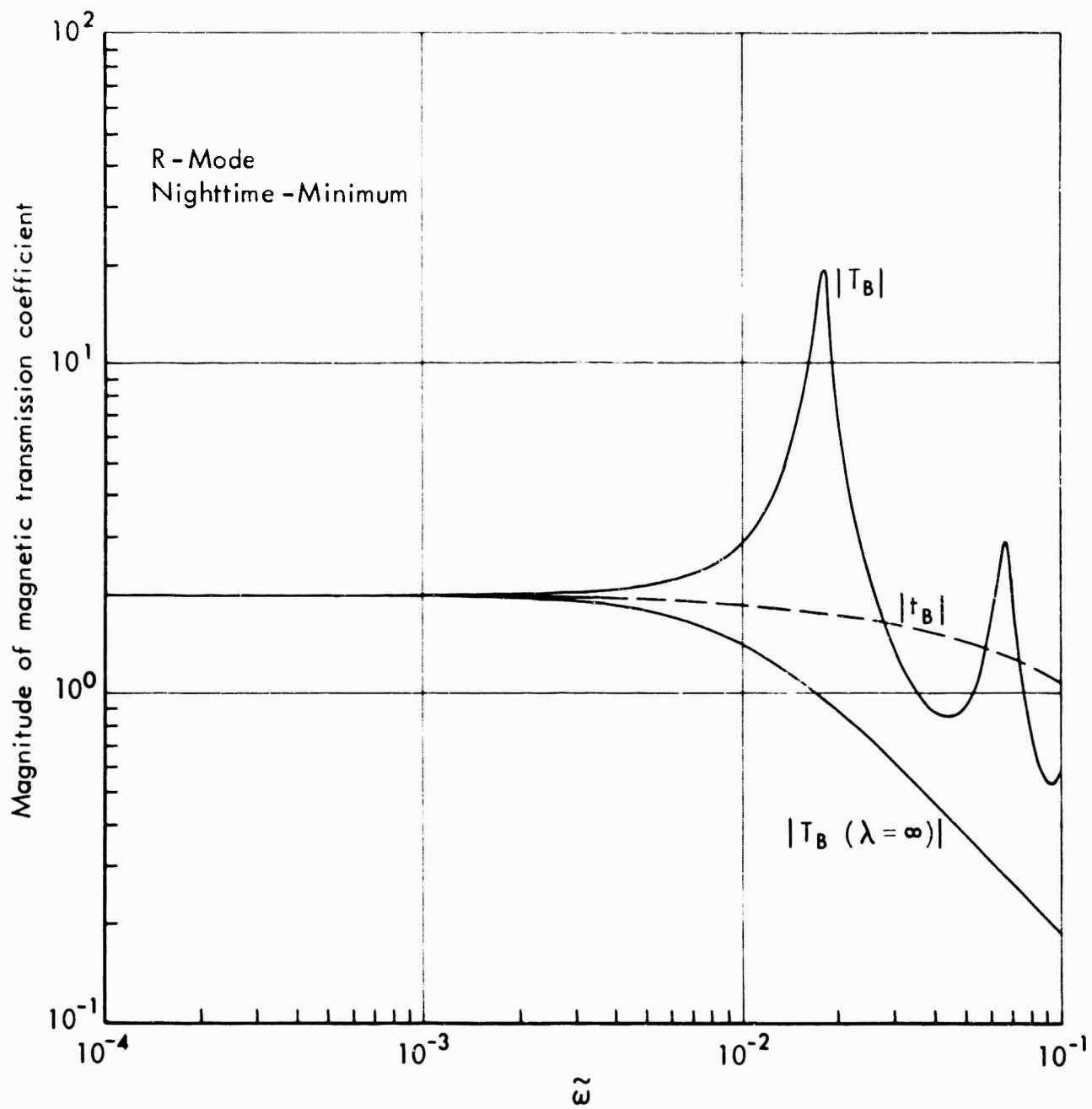


Fig. 7

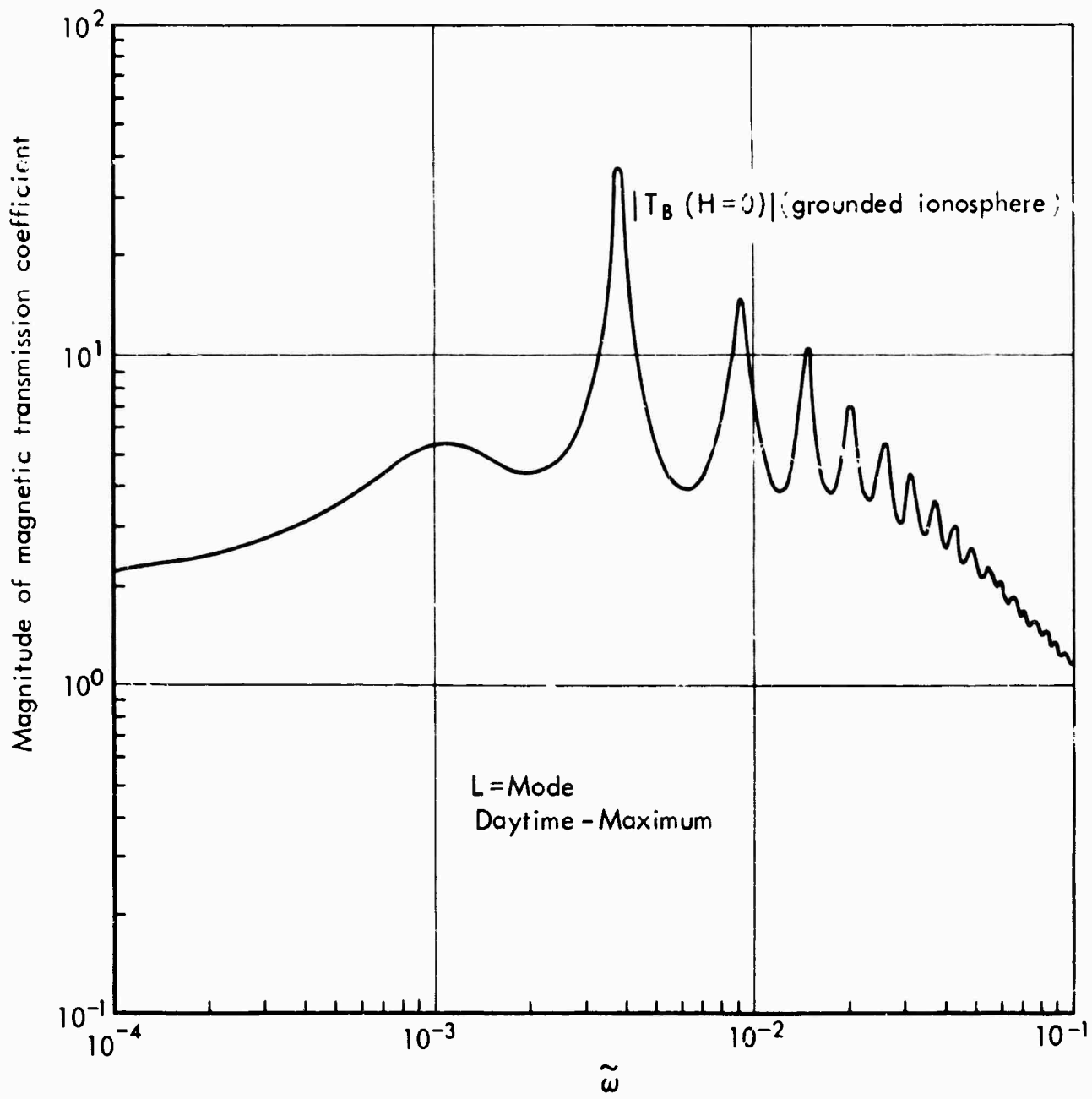


Fig. 8

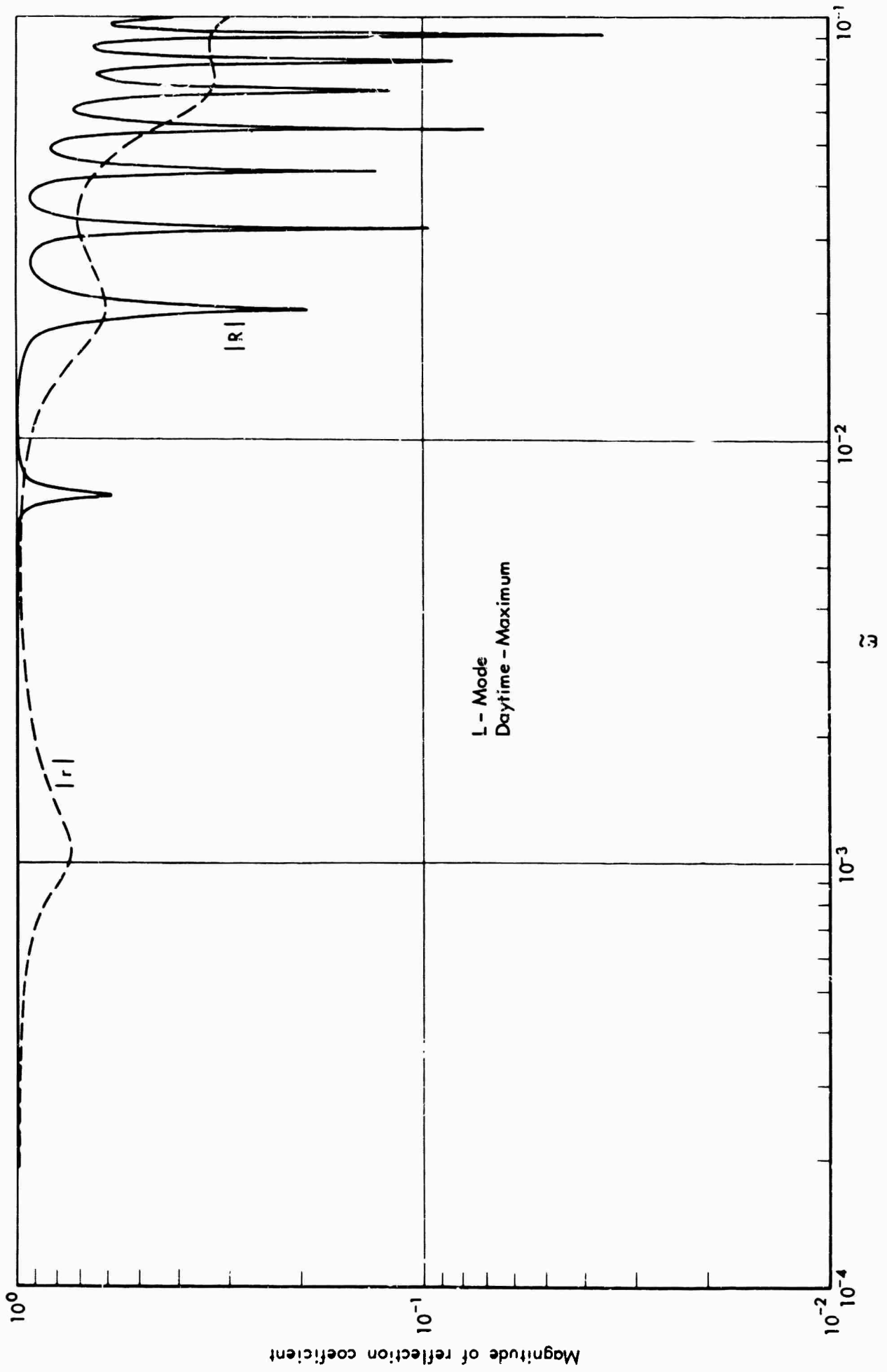


Fig. 9

REFERENCES

1. Benioff, H., "Observations of Geomagnetic Fluctuations in the Period Range 0.3 to 120 Seconds," J. Geophys. Res., 65, 1413-1435, 1960.
2. Davidson, M.J., "Average Diurnal Characteristics of Geomagnetic Power Spectrums in the Period Range 4.5 to 1000 Seconds," J. Geophys. Res., 69, 5116-5119, 1964.
3. Elliott, R.D., and Hodder, D.T., "On a Local Generation Model for Geomagnetic Micropulsations Caused by High-Altitude Weapons Tests," North American Aviation Co., 1965 (to be published).
4. Francis, W.E., and R. Karplus, "Hydromagnetic Waves in the Ionosphere," J. Geophys. Res., 65, 3593-3600, 1960.
5. Greifinger, C. and P. Greifinger, "Transmission of Micropulsations Through the Lower Ionosphere," J. Geophys. Res., 1965 (to be published) and The RAND Corporation, RM-4388, 1964.
6. Jacobs, J.A. et al., "Classification of Geomagnetic Micropulsations," J. Geophys. Res., 69, 180-181, 1964.
7. Jacobs, J.A., and T. Watanabe, "Propagation of Hydromagnetic Waves in the Lower Exosphere and the Origin of Short Period Geomagnetic Micropulsations," J. Atmos. Terrest. Phys., 24, 413-434, 1962.
8. Maple, E., "Geomagnetic Oscillations at Middle Latitudes," J. Geophys. Res., 63, 1395-1404, 1959.
9. Ness, N.F., et al., "Magnetic Field Fluctuations on the Earth and in Space," Jour. Phys. Soc. of Japan, 17 supplement A-II, 27-33, 1962.
10. Prince, C.E., and F.X. Bostick, "Ionospheric Transmission of Transversely Propagated Plane Waves at Micropulsation Frequencies and Theoretical Power Spectrums," J. Geophys. Res., 69, 3213-3234, 1964.
11. Santirocco, R.A., and D.G. Parker, "The Polarization and Power Spectrums of Pc Micropulsations in Bermuda," J. Geophys. Res., 68, 5545-5558, 1963.
12. Smith, H.W., L.D. Provazek and F.X. Bostick, "Directional Properties and Phase Relations of the Magnetotelluric Fields at Austin, Texas," J. Geophys. Res., 66, 879-888, 1961.
13. Tepley, L.R., "Observations of Hydromagnetic Emissions," J. Geophys. Res., 66, 1651-1658, 1961.

14. Tepley, L., and Amundsen, K.D., "Observations of Continuous Sub-ELF Emissions in the Frequency Range 0.2 to 1.0 Cycles per Second," J. Geophys. Res., 70, 234-239, 1965.